

## Lattice dynamics of $\text{YBa}_2\text{Cu}_3\text{O}_7$

Hanae Nozaki and Satoshi Itoh

*Advanced Research Laboratory, Research and Development Center, Toshiba Corporation, 1, Komukai Toshiba-cho, Saiwai-ku, Kawasaki 210, Japan*

(Received 25 March 1993)

The lattice vibration of  $\text{YBa}_2\text{Cu}_3\text{O}_7$  is investigated based on a distributed-multipole model. In this model, the interatomic potential is expressed by means of a multipole-multipole interaction. The dipole and quadrupole moments are taken into account as higher-order multipole moments in order to include structural anisotropy in  $\text{YBa}_2\text{Cu}_3\text{O}_7$ . The quadrupole moments, as compared with the dipole moments, play an important role in the structural stability of this material. The phonon-dispersion relation and the density of states are calculated. The obtained neutron-weighted density of states gives good agreement with the experimental phonon spectrum. The relation between the vibrational properties of the oxygen atoms and the structural  $a$ - $b$  anisotropy is discussed.

### I. INTRODUCTION

The high- $T_c$  superconductor  $\text{YBa}_2\text{Cu}_3\text{O}_7$  has a complex crystal structure, in which the  $\text{CuO}_2$  planes are stacked along the  $c$  axis and the  $\text{CuO}_3$  chain runs along the  $b$  axis.<sup>1</sup> The  $\text{CuO}_3$  chain structure gives a structural  $a$ - $b$  anisotropy, which cannot be obtained in the nonsuperconductor  $\text{YBa}_2\text{Cu}_3\text{O}_6$ . There is a remarkable difference in the lattice vibration between these two materials because of this structural anisotropy. Renker *et al.*<sup>2</sup> reported that experimental phonon spectra of  $\text{YBa}_2\text{Cu}_3\text{O}_{7-\delta}$  are substantially changed with varying  $\delta$  from 0 to 1. Since the phonons make some contribution to the mechanism of high- $T_c$  superconductivity, several theoretical investigations on the lattice vibration in  $\text{YBa}_2\text{Cu}_3\text{O}_{7-\delta}$  have been carried out using empirical models, such as rigid-ion models,<sup>3-6</sup> shell models,<sup>7-10</sup> and a valence-bond force field model.<sup>11</sup> For complex-structured materials such as  $\text{YBa}_2\text{Cu}_3\text{O}_7$ , the use of empirical models has an advantage of saving much computational time. It is rather difficult for first-principles calculations to treat systems containing defects or impurities. For these reasons, empirical calculations are needed for such complex systems.

The crystal structure of  $\text{YBa}_2\text{Cu}_3\text{O}_7$  is shown in Fig. 1. The labeling of the atoms refers to the notation of Siegrist *et al.*<sup>12</sup> The unit cell is orthorhombic and the space group is  $P_{mmm}$ .<sup>1</sup> The atoms Cu(2), O(2), and O(3) form the  $\text{CuO}_2$  plane, and the atoms Cu(1), O(1), and O(4) form the  $\text{CuO}_3$  chain. The O(4) atoms along the  $b$  axis cause the structural  $a$ - $b$  anisotropy.

A reliable interatomic model potential is required to calculate the lattice vibration. It is desirable that the model potential provides the same stable crystal structures as the observed ones. This condition, however, cannot always be satisfied for complex-structured materials. In particular, there is the strong structural anisotropy in  $\text{YBa}_2\text{Cu}_3\text{O}_7$ , so that the crystal structure of  $\text{YBa}_2\text{Cu}_3\text{O}_7$  is difficult to be stabilized by means of simple models such as rigid-ion models.

Chaplot<sup>3</sup> studied the crystal structure of  $\text{YBa}_2\text{Cu}_3\text{O}_7$  based on the rigid-ion model. He reported that, in the equilibrium structure of  $\text{YBa}_2\text{Cu}_3\text{O}_7$ , the atomic positions of Ba and O(1) in fractional coordinates differ from experimental values by 4 and 6%, respectively. Wright and Butler<sup>6</sup> investigated the structures of the Y-Ba-Cu family of oxides by means of an extended rigid-ion model. In this model, a three-body potential to represent the O—Cu—O bond angle was introduced as an additional term. They pointed out that the additional term plays an essential role to stabilize the structures of these materials, and, also, that a dipole-dipole interaction is not adequate for stabilizing the crystal structures.

In this paper, we propose a model of empirical interatomic potentials for complex-structured materials and calculate the lattice vibration of  $\text{YBa}_2\text{Cu}_3\text{O}_7$ . This model, the distributed-multipole model (DMM), takes into account the multipole-multipole interaction to deal with structural anisotropy. In the DMM, the interatomic potential is given by interactions between multipole moments located at each atomic site. The higher-order mul-

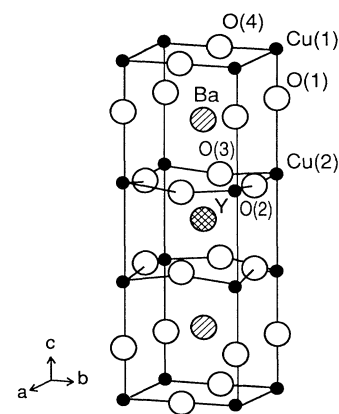


FIG. 1. A unit cell of the  $\text{YBa}_2\text{Cu}_3\text{O}_7$  crystal structure. The atoms are labeled according to the notation of Ref. 12.

tipole moments correspond to the distortion of the spherical charge distribution at each atom. The aim of this paper is to find out how accurately we can calculate the structure of  $\text{YBa}_2\text{Cu}_3\text{O}_7$  by including such higher-order multipoles. The DMM can be applied to various materials from ionic to covalent materials, since anisotropic interactions are involved in the interatomic potential. Moreover, the relations between lattice vibration and structural anisotropy can be discussed based on the calculated results for lattice dynamics.

This paper is organized as follows: In the next section, the interatomic potential based on the DMM and an estimation procedure for the potential parameters are described. In Sec. III, we report the calculated equilibrium structure of  $\text{YBa}_2\text{Cu}_3\text{O}_7$  and discuss the roles of the higher-order multipole moments in structural stability. In Sec. IV, the calculated results of the phonon-dispersion relation and the neutron-weighted density of states (DOS) are compared with experimental data. Furthermore, in the calculation of the partial DOS's, we give some discussions on the  $a$ - $b$  anisotropy in the vibrations of each oxygen atom. Finally, a short summary is given in Sec. V.

## II. INTERATOMIC POTENTIAL

The interaction between the point charges is regarded as a leading term in interatomic interaction, since ionic

bonds play primary roles in the chemical bonds of  $\text{YBa}_2\text{Cu}_3\text{O}_7$ . The structural anisotropy of this material, however, indicates that ionicity and covalency are coexistent. Higher-order moments given by a multipole expansion of the charge distribution are taken into account in the DMM to describe structural anisotropy. The interatomic potential based on this model is described by the interactions between multipoles located at each atomic site. The values of these multipole moments are determined through the equilibrium conditions for the crystal.

In the DMM, the interatomic potential between the atoms  $s$  and  $s'$  can be divided into two terms by the following expression:

$$\phi(ss') = \phi^R(ss') + \phi^M(ss'), \quad (1)$$

where  $\phi^R$  is the short-range repulsive potential and  $\phi^M$  is the multipole-multipole interaction. The term  $\phi^R$  is a Born-Mayer-type potential:

$$\phi^R(ss') = A \exp \left[ -B \frac{r^{(ss')}}{R^{(s)} + R^{(s')}} \right], \quad (2)$$

where  $r^{(ss')}$  is the distance between the  $s$ th and  $s'$ th atoms and  $R^{(s)}$  is the effective radius of the  $s$ th atom. The constants  $A$  and  $B$  are 1822 eV and 12.364, respectively.<sup>3</sup> As the multipole moments are summed up to  $L$ th order,  $\phi^M$  is written in the following form:<sup>13,14</sup>

$$\phi^M(ss') = \frac{e^2}{4\pi\epsilon_0} \sum_{l=0}^L \sum_{l'=0}^L \frac{(-1)^l}{(2l-1)!!(2l'-1)!!} \sum_{i[l]} \sum_{i'[l']} M_{i[l]}^{(s)} M_{i'[l']}^{(s')} \left[ \nabla_{i[l]} \nabla_{i'[l']} \frac{1}{r^{(ss')}} \right], \quad (3)$$

with  $(2l-1)!! = (2l-1)(2l-3) \cdots 1$  and

$$\nabla_{i[l]} \equiv \frac{\partial^l}{\partial r_i \partial r_j \cdots}. \quad (4)$$

The symbol  $M_{i[l]}^{(s)}$  corresponding to the  $l$ th-order multipole moment  $M_{ij}^{(s)} \dots$  is defined by

$$M_{i[l]}^{(s)} = \frac{(-1)^l}{l!} \int \rho^s(\mathbf{r}) r^{2l+1} \left[ \nabla_{i[l]} \frac{1}{r} \right] d\mathbf{r}, \quad (5)$$

where  $\rho^s(\mathbf{r})$  is the charge distribution of the  $s$ th atom. Since Eq. (5) satisfies the condition

$$\sum_i M_{ijk \dots}^{(s)} = 0, \quad (6)$$

the degree of freedom by the  $l$ th-order multipole moment is  $2l+1$ . The Ewald method is used for the lattice sums of the multipole-multipole interaction.<sup>13,15,16</sup>

In this paper, multipoles up to the second order are taken into account. The monopole (point charge), dipole moment, and quadrupole moment are denoted by  $Z$ ,  $P_i$ , and  $Q_{ij}$ , respectively. Then, the set of potential parameters in this paper is composed of  $R^{(s)}$ ,  $Z^{(s)}$ ,  $P_i^{(s)}$ , and  $Q_{ij}^{(s)}$ . The charge neutrality condition of the unit cell is required as for  $Z^{(s)}$ .

Although the present DMM contains many potential parameters, some of them are restricted in their degree of

freedom because of the space group symmetry. In the case of  $\text{YBa}_2\text{Cu}_3\text{O}_7$ , the following restrictions are imposed on  $P_i^{(s)}$  and  $Q_{ij}^{(s)}$ . As for the dipole moments, only  $P_z^{(s)}$  (component along the  $c$  axis) can be located at the atomic sites: Ba, Cu(2), O(1), O(2), and O(3), while any dipole moments are forbidden at the other sites: Y, Cu(1), and O(4). On the other hand, as for the quadrupole moments, three components  $Q_{xx}^{(s)}$ ,  $Q_{yy}^{(s)}$ , and  $Q_{zz}^{(s)}$  can be located at all atomic sites. Considering the strict restriction on the dipole moments, we expect that the dipole moments contribute little to the interatomic interaction of  $\text{YBa}_2\text{Cu}_3\text{O}_7$ . Compared with the dipole moments, the quadrupole moments have a relatively higher degree of freedom. From the analysis on space group symmetry, only the quadrupole moments are effective higher-order moments to represent the structural anisotropy of  $\text{YBa}_2\text{Cu}_3\text{O}_7$ .

A crystal structure is generally specified by structural parameters, i.e., the lattice constants ( $a$ ,  $b$ ,  $c$ ,  $\alpha$ ,  $\beta$ , and  $\gamma$ ) and the fractional atomic coordinates. Structural parameters are divided into two groups according to whether changes in their values change the space group symmetry. The structural parameter maintaining the original space group symmetry is denoted by  $\xi_\alpha$  hereafter. In the case of  $\text{YBa}_2\text{Cu}_3\text{O}_7$ , the parameters  $\xi_\alpha$  are the lattice constants  $a$ ,  $b$ , and  $c$  and the fractional  $z$  coordinates of Ba,

TABLE I. Potential parameters of  $\text{YBa}_2\text{Cu}_3\text{O}_7$  in the DMM.

	Y	Ba	Cu(1)	Cu(2)	O(1)	O(2)	O(3)	O(4)
$R^{(s)}$ (Å)	1.844	2.248	1.197	1.245	1.556	1.749	1.747	1.805
$Z^{(s)}$	2.075	1.537	1.122	1.376	-1.052	-1.380	-1.390	-1.379
$P_z^{(s)}$ (Å)		-0.025		0.023	0.049	-0.075	-0.072	
$Q_{xx}^{(s)}$ (Å <sup>2</sup> )	-0.009	0.016	-0.275	0.091	0.079	-0.122	0.063	0.069
$Q_{yy}^{(s)}$ (Å <sup>2</sup> )	-0.006	0.014	0.142	0.097	0.080	0.059	-0.128	-0.139
$Q_{zz}^{(s)}$ (Å <sup>2</sup> )	0.015	-0.030	0.133	-0.188	-0.159	0.063	0.065	0.070

Cu(2), O(1), O(2), and O(3). Then, the equilibrium condition for the crystal is given by

$$\left. \frac{\partial W_{\text{total}}}{\partial \xi_\alpha} \right|_{\xi_\alpha = \xi_\alpha^{\text{expt}}} = 0, \quad (7)$$

where  $W_{\text{total}}$  is the total potential energy and  $\xi_\alpha^{\text{expt}}$  represents an experimental value.<sup>17</sup> A set of potential parameters satisfying Eq. (7) is obtained by means of the nonlinear least-squares method.<sup>18</sup>

### III. STRUCTURAL STABILITY

The potential parameters of  $\text{YBa}_2\text{Cu}_3\text{O}_7$  obtained by the above-mentioned procedure are given in Table I. And, based on these parameters, the calculated equilibrium structure of  $\text{YBa}_2\text{Cu}_3\text{O}_7$  is given in Table II. It is in fairly good agreement with the experimental structures<sup>19-21</sup> and its deviations from these experimental values are reduced to less than 1% for all structural parameters. The total potential energy per unit cell is -124.9 eV and is divided into the following contributions: The repulsive energy coming from the Born-Mayer-type potential is 17.6 eV. The remainder, -142.5 eV, originates from the multipole-multipole interaction, and 97% of this interaction is caused by the monopole-monopole interaction. The energies by the dipole-dipole, quadrupole-quadrupole, monopole-dipole, and monopole-quadrupole interactions are 0.03, -0.3, 0.2, and -4.3 (eV), respectively. The contribution from the dipole-quadrupole interaction is sufficiently small to be negligible.

In the present DMM, the contribution from the higher-order terms in the multipole-multipole interaction, which is neglected in the rigid-ion model, is included. The calculated equilibrium structure based on the

DMM gives good agreement with the experimentally observed one, so that the higher-order terms play an important role in the structural stability of  $\text{YBa}_2\text{Cu}_3\text{O}_7$ . Among the higher-order terms, the quadrupole moments contribute more largely than the dipole moments from the reasons mentioned below. Since the local structures around the Cu(1) and O(4) sites are anisotropic, a large amount of the multipole moment is expected to exist for the Cu(1) and O(4) sites. These atomic sites, however, are prohibited by the constraint of space group symmetry to have any dipole moments. Therefore, these anisotropic structures around the Cu(1) and O(4) sites should be stabilized by the quadrupole moments positioned at these atomic sites. The characteristic  $\text{CuO}_3$  chain structure in  $\text{YBa}_2\text{Cu}_3\text{O}_7$  implies the presence of large quadrupole moments. A few tests were carried out to further check the contribution of the quadrupole moments, and the following results were obtained: If the quadrupole moments are completely neglected, it is difficult to stabilize the structure having the experimental structural parameters. In contrast, even if the dipole moments are completely neglected, almost the same results for  $Z^{(s)}$  and  $Q_{ij}^{(s)}$  as shown in Table I can be obtained, and the calculated equilibrium structure satisfactorily agrees with the experimental one. Wright and Butler<sup>6</sup> indicated that the use of a dipole-dipole interaction as an additional term cannot stabilize the structure of  $\text{YBa}_2\text{Cu}_3\text{O}_7$ , which is consistent with the present numerical result. From the viewpoint of energetic analysis, the contribution from the higher-order terms to the multipole-multipole interaction energy is only 3%, and most of the total potential energy arises from the monopole-monopole interaction. It is reasonable that the physical properties such as phonon frequencies are almost determined by the value of  $Z^{(s)}$ , as will be discussed in the next section. Nevertheless, the contribution from the higher-order terms is significant to provide structural stability.

TABLE II. Calculated and experimental structures of  $\text{YBa}_2\text{Cu}_3\text{O}_7$ .

	Lattice constants (Å)			Fractional $z$ coordinates				
	$a$	$b$	$c$	Ba	Cu(2)	O(1)	O(2)	O(3)
Calculated	3.820	3.880	11.700	0.185	0.356	0.157	0.379	0.379
Observed <sup>a</sup>	3.820	3.885	11.683	0.184	0.355	0.158	0.378	0.377
Observed <sup>b</sup>	3.819	3.883	11.669	0.184	0.355	0.158	0.379	0.377
Observed <sup>c</sup>	3.810	3.883	11.674	0.185	0.357	0.158	0.377	0.380

<sup>a</sup>Reference 19.

<sup>b</sup>Reference 20.

<sup>c</sup>Reference 21.

#### IV. LATTICE VIBRATION

The calculated phonon-dispersion relation for  $\text{YBa}_2\text{Cu}_3\text{O}_7$  along the directions  $[\xi 0 0]$ ,  $[0 \xi 0]$ ,  $[\xi \xi 0]$ , and  $[0 0 \xi]$  in the Brillouin zone are shown in Fig. 2. Since the unit cell of  $\text{YBa}_2\text{Cu}_3\text{O}_7$  contains 13 constituent atoms, 39 vibrational modes are obtained. The calculated phonon frequencies have no imaginary value all over the Brillouin zone, which means that the dynamical matrix is positive definite for all  $\mathbf{q}$  points. This result means that the DMM is capable of calculating the lattice vibration by using the potential parameters obtained from the static condition.

The experimental dispersion relation<sup>22</sup> obtained by an inelastic-neutron-scattering measurement is also shown in Fig. 2. Since a twinned crystal was used in the experiment, the observed dispersion relations along the  $[\xi 0 0]$  and  $[0 \xi 0]$  directions cannot be distinguished between each other. Although all vibrational modes have not been detected experimentally, the calculated result is not inconsistent with the observed one. The gradients of the longitudinal acoustic modes at the  $\Gamma$  point are sound velocities. The calculated longitudinal sound velocities are  $5.25 \times 10^5$  cm/s along the  $[\xi 0 0]$  direction and  $4.08 \times 10^5$  cm/s along the  $[0 0 \xi]$  direction. The experimental values for these velocities are  $6.47 \times 10^5$  and  $4.52 \times 10^5$  cm/s, respectively. In this paper, multipole moments induced by the vibrations are not taken into account. It is known that such induced multipole moments lower the frequency of the optic modes in the region of long wavelength.<sup>23</sup> There is a possibility that the calculated highest optic

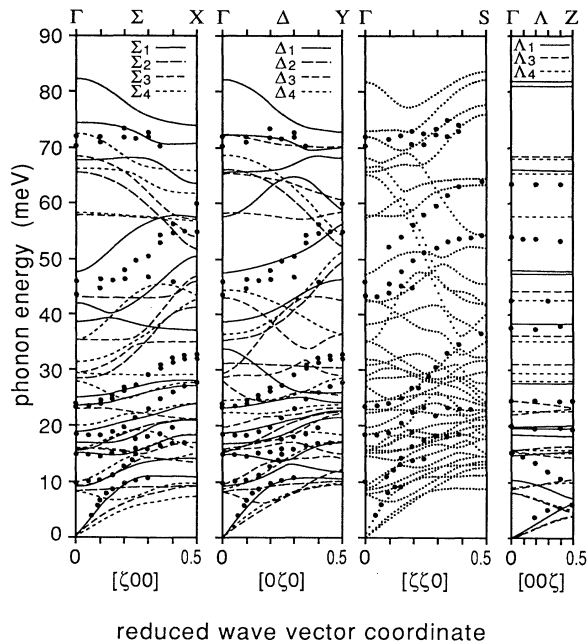


FIG. 2. The calculated dispersion curves of  $\text{YBa}_2\text{Cu}_3\text{O}_7$  along four symmetry directions in the Brillouin zone using the DMM. Closed circles indicate experimental data by means of inelastic neutron scattering by Reichardt *et al.* (Ref. 22). See text for details.

mode near the  $\Gamma$  point decreases by the consideration of the induced multipole moments and, consequently, agreement with the experimental result will be improved. In Ref. 22, the dispersion relations are obtained by connecting the measured points with lines. As compared with these experimental dispersion curves, the present calculated dispersion curves in the lower-energy region below 40 meV are rather flat with a wave vector. Except for the longitudinal acoustic modes, there is no obvious one-to-one correspondence between the experimental and calculated curves. It, however, seems that the measured points assigned to one experimental curve belong to several calculated curves. In other words, the experimental dispersion curves transverse several calculated dispersion curves specified by the same irreducible representation. Since the present calculated result shows that most of the 39 vibrational modes are concentrated in the lower-energy region below 40 meV, it is difficult to distinguish branches having the same symmetry.

The calculated neutron-weighted DOS of  $\text{YBa}_2\text{Cu}_3\text{O}_7$  is shown in Fig. 3. This spectrum depends on the choice of the neutron-scattering weight factor which is the total scattering cross section divided by the mass. The values of these factors for Y, Ba, Cu, and O are 0.0849, 0.0252, 0.1178, and 0.2647 (b/amu), respectively.<sup>3,24</sup> We have calculated the phonon spectrum with 125  $\mathbf{q}$  points in the irreducible Brillouin zone and broadened each vibrational level with Gaussian functions of the full width at half maximum of 3.3 meV. As shown in Fig. 3, the calculated phonon spectrum is in good agreement with the experimental spectrum by Renker *et al.*<sup>2</sup> for the bandwidth and all peak positions except for the calculated peak position at 65 meV. Recently, Arai *et al.*<sup>25</sup> measured the phonon DOS of  $\text{YBa}_2\text{Cu}_3\text{O}_7$  in detail. The present calculated phonon spectrum also agrees with that experimental spectrum, but does not have a peak corresponding to the measured peak at 87 meV in Ref. 25. The origins of the calculated peaks will be discussed later.

As presented in Table I, the fitted potential parameters  $Z^{(s)}$  show considerably smaller absolute values than the closed-shell ions ( $Z^{(\text{Y})}=3$ ,  $Z^{(\text{Ba})}=2$ ,  $Z^{(\text{Cu})}=2$ , and  $Z^{(\text{O})}=-2$ ). The lattice dynamics was calculated using nearly closed-shell values ( $Z^{(\text{Y})}=2.4$ ,  $Z^{(\text{Ba})}=2.05$ ,  $Z^{(\text{Cu})}=1.9$ ,  $Z^{[\text{O}(1),\text{O}(4)]}=-1.8$ , and  $Z^{[\text{O}(2),\text{O}(3)]}=-1.7$ )

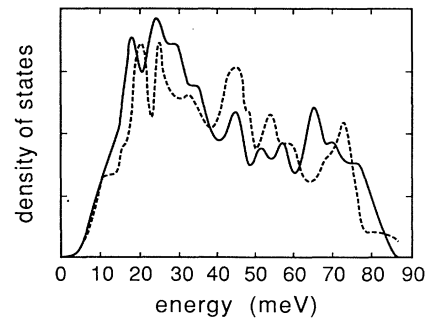


FIG. 3. The calculated neutron-weighted density of states of  $\text{YBa}_2\text{Cu}_3\text{O}_7$  (solid line), together with the experimental phonon spectrum (dashed line) obtained from inelastic neutron scattering by Renker *et al.* (Ref. 2).

to examine the contribution of  $Z^{(s)}$  to the phonon spectrum. As a result, the calculated spectrum disagreed with the experimental neutron-weighted spectrum. The calculated bandwidth increased by nearly 20% as compared with that of the spectra shown in Fig. 3. Furthermore, some of the calculated vibrational modes had imaginary frequencies, which indicates that the dynamical matrix in this case does not always become positive definite in the whole Brillouin zone. These results can be explained by the following reasons: A small increase in the absolute values of  $Z^{(s)}$  causes a considerable increase in the phonon frequencies, since most of the total potential energy is given by the monopole-monopole interaction. In the DMM, the higher-order multipole moments have an effect on the structural stability. This effect of the higher-order multipoles decreases and the crystal structure becomes unstable when the absolute values of  $Z^{(s)}$  are too large. It is, therefore, reasonable that the potential parameters  $Z^{(s)}$  should have smaller absolute values than the closed-shell ions. This result supports the fact that  $\text{YBa}_2\text{Cu}_3\text{O}_7$  is an ionicity and covalency coexisting system. Although the values of the obtained potential parameters do not correspond to the actual physical quantity in the present estimation procedure, the potential parameters given in Table I are adequately reflected by the physical situation in this system.

The partial DOS's are discussed below for a detailed analysis on the neutron-weighted spectrum. The calculated results of the partial DOS's for the individual elements are presented in Fig. 4(a). It has been found that only the oxygen atoms vibrate in the higher-energy region above 40 meV. This fact is caused by the lightest mass of the oxygen atom among the four constituent ele-

ments. The neutron-weighted spectrum in the higher-energy region mostly originates from the vibrations of the oxygen atoms, so that the feature of the spectrum in this energy region is sensitive to local structural changes at the oxygen atom site as a defect. The structural  $a$ - $b$  anisotropy in  $\text{YBa}_2\text{Cu}_3\text{O}_7$  is caused by the oxygen atoms. In Fig. 2, the  $a$ - $b$  anisotropy in the lattice vibration consequently appears in the higher-energy region. Unfortunately, this  $a$ - $b$  anisotropy expected in the dispersion relation of  $\text{YBa}_2\text{Cu}_3\text{O}_7$  has not been observed because of the use of a twinned crystal in the measurement.<sup>22</sup> In the lower-energy region, the neutron-weighted spectrum is affected by vibrations of the copper atoms in addition to the oxygen atoms. In Fig. 3, the calculated large peaks at 18 and 23 meV mainly come from vibrations of the oxygen and copper atoms. A shoulder structure at about 14 meV seen in Fig. 3 is caused by the barium atoms. This contribution forms not a peak but a shoulder because the neutron-scattering weight factor for the barium atom is small. From the same reason, a contribution from the yttrium atoms is also small.

The calculated results of the partial DOS's for the individual oxygen atoms are shown in Fig. 4(b). The characteristics of lattice dynamics in  $\text{YBa}_2\text{Cu}_3\text{O}_7$  are specified by vibrations of the oxygen atoms. The vibrational modes of the individual oxygen atoms are discussed in relation to the  $a$ - $b$  anisotropy in the following paragraphs.

First, the partial DOS of O(1) has a large peak centered at about 32 meV. The vibrational modes of the O(1) atoms along the  $a$  and  $b$  directions are equivalent in  $\text{YBa}_2\text{Cu}_3\text{O}_6$  because of the tetragonal symmetry in its unit cell. The vibrational modes of the O(1) atoms in  $\text{YBa}_2\text{Cu}_3\text{O}_7$ , however, show a relatively large  $a$ - $b$  anisotropy because of the presence of the O(4) atoms. In the present calculation, the vibrations of the O(1) atoms along the  $a$  direction contribute to a large peak at about 30 meV but have no significant contribution in the higher-energy region above 50 meV. On the other hand, the vibrations of the O(1) atoms along the  $b$  direction have frequencies of the energy widely ranged from 20 to 70 meV. In the energy region around 50 meV, it has been found that almost only the O(1) atoms are vibrating along the  $b$  direction in the  $\text{CuO}_3$  chain. Such vibrations of the O(1) atoms are expected to disappear in  $\text{YBa}_2\text{Cu}_3\text{O}_6$ , since this vibration is attributed to the structural  $a$ - $b$  anisotropy. It has been experimentally reported that the phonon spectrum intensity of  $\text{YBa}_2\text{Cu}_3\text{O}_{7-\delta}$  in the intermediate-energy region decreases remarkably with varying  $\delta$  from 0 to 1.<sup>2</sup> It seems that this change in the spectrum is related to the above-mentioned vibration of the O(1) atoms.

Next, let us discuss the vibrations of oxygen atoms in the  $\text{CuO}_2$  plane. From Fig. 4(b), the partial DOS's of O(2) and O(3) mainly determine the neutron-weighted spectrum bandwidth. The force constants in this plane are relatively large, since the potential function in the  $a$ - $b$  plane is rather rapidly changing spatially. Therefore, the vibrations of the O(2) and O(3) atoms in the  $a$ - $b$  plane have high frequencies and contribute mainly to the higher-energy region above 60 meV in the neutron-weighted spectrum. The partial DOS of O(2) is very close

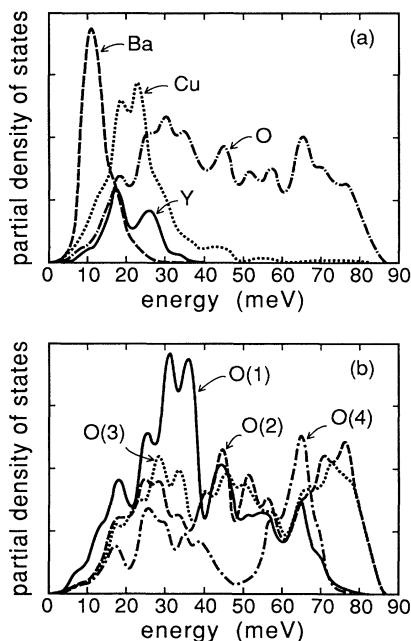


FIG. 4. The calculated partial density of states of  $\text{YBa}_2\text{Cu}_3\text{O}_7$  (a) for the individual elements and (b) for the individual oxygen atoms.

to that of O(3) except for the energy region from 20 to 40 meV. In this energy region, the partial DOS of O(1) has the large peak structure. The difference between the spectra of O(2) and O(3) can be attributed to the *a-b* anisotropy through the vibrations of the O(1) atoms, since the vibrations of the O(1) atoms strongly affected by the structural *a-b* anisotropy.

Lastly, the partial DOS of O(4) is mainly constructed with two large peaks centered at 26 and at 65 meV, and there is a large dip structure at about 50 meV. This spectrum of O(4) is explained by the anisotropic local potential around the O(4) site. The force constant of O(4) along the *a* direction is rather small, since the local potential around the O(4) site gradually changes along this direction. Therefore, the vibrations of the O(4) atoms along the *a* direction have low frequencies. On the other hand, there is the chain structure —O(4)—Cu(1)—O(4)—Cu(1)— along the *b* direction. Since the potential along this chain direction rapidly changes spatially, the vibrational modes along the *b* direction have high frequencies. These vibrational modes correspond to the bond-stretching modes. Thus, the lower-energy part and the higher-energy part in the partial DOS of O(4) mainly come from the bond-bending modes and the bond-stretching modes, respectively.

## V. CONCLUSIONS

In the present paper, we have proposed the DMM as a reasonable model of empirical interatomic potentials for complex-structured materials such as the high- $T_c$  superconductor  $\text{YBa}_2\text{Cu}_3\text{O}_7$ . The DMM is characterized by its anisotropic potential function given by the multipole-multipole interaction. In the present calculation for  $\text{YBa}_2\text{Cu}_3\text{O}_7$ , the dipole and quadrupole moments have been taken into account as higher-order multipole moments. The calculated equilibrium structure is in fairly good agreement with the experimental one. This result indicates that the DMM is capable of dealing with the structural anisotropy of  $\text{YBa}_2\text{Cu}_3\text{O}_7$ . The quadrupole moments are important for the structural stability of this material. Owing to these moments, the O(4) atoms are prevented from moving toward the *a* direction and the —O(4)—Cu(1)—O(4)—Cu(1)— chain structure becomes stable. The dipole moments, in contrast to the quadru-

pole moments, contribute little to the interatomic interaction in  $\text{YBa}_2\text{Cu}_3\text{O}_7$ . This difference between the dipole and quadrupole moments is attributed to the restriction from space group symmetry. From the present calculated results, it has been concluded that the multipole-multipole interaction plays an important role in the interatomic interactions in anisotropic materials. In the DMM, no additional term is needed in order to stabilize anisotropic structures. It is possible that the DMM is applicable to various complex-structured materials.

The lattice dynamics of  $\text{YBa}_2\text{Cu}_3\text{O}_7$  have been calculated by using the DMM. From the calculated results of the phonon-dispersion relation, it has been found that the dynamical matrix becomes positive definite for all  $\mathbf{q}$  points in the Brillouin zone. The potential parameters obtained from the equilibrium condition are applicable to the calculation of lattice dynamics. The calculated neutron-weighted DOS gives good agreement with the experimental one for both the bandwidth and the peak positions. From the calculated partial DOS's, it has been found that the vibrations of the oxygen atoms show a remarkable *a-b* anisotropy. Under the influence of the multipole moments positioned at the O(4) sites, the vibrations of the O(1) atoms along the *a* direction are restricted to have high energy above 50 meV. In the energy region around 50 meV, almost only the O(1) atoms are vibrating along the *b* direction in the  $\text{CuO}_3$  chain. In the partial DOS's of the oxygen atoms in the  $\text{CuO}_2$  plane, the *a-b* anisotropy particularly appears in the intermediate-energy region. The partial DOS of the O(4) atoms splits into two peaks. These peaks in the lower-energy region and in the higher-energy region are caused by the vibrations along the *a* and *b* directions, respectively. If the phonons contribute to the mechanism of high- $T_c$  superconductivity, such *a-b* anisotropy in the lattice vibration may have some effects on this mechanism. It is required to measure more branches in the phonon-dispersion relation by using single crystals, together with theoretical approaches.

## ACKNOWLEDGMENTS

We would like to thank K. Ando, K. Kato, and S. Tanaka of the TOSHIBA Corporation for their helpful discussions and critical readings of this manuscript.

- 
- <sup>1</sup>J. E. Greedan, A. H. O'Reilly, and C. V. Stager, Phys. Rev. B **35**, 8770 (1987).  
<sup>2</sup>B. Renker, F. Gompf, E. Gering, D. Ewert, H. Rietschel, and A. Dianoux, Z. Phys. B **73**, 309 (1988).  
<sup>3</sup>S. L. Chaplot, Phys. Rev. B **37**, 7435 (1988).  
<sup>4</sup>P. A. Deymier, Phys. Rev. B **38**, 6596 (1988).  
<sup>5</sup>S. L. Chaplot, Phys. Rev. B **42**, 2149 (1990).  
<sup>6</sup>N. F. Wright and W. H. Butler, Phys. Rev. B **42**, 4219 (1990).  
<sup>7</sup>C. Thomsen, M. Cardona, W. Kress, R. Liu, L. Genzel, M. Bauer, E. Schönherr, and U. Schröder, Solid State Commun. **65**, 1139 (1988).  
<sup>8</sup>R. Liu, C. Thomsen, W. Kress, M. Cardona, B. Gegenheimer, F. W. de Wette, J. Prade, A. D. Kulkarni, and U. Schröder, Phys. Rev. B **37**, 7971 (1988).  
<sup>9</sup>W. Kress, U. Schröder, J. Prade, A. D. Kulkarni, and F. W. de Wette, Phys. Rev. B **38**, 2906 (1988).  
<sup>10</sup>R. C. Baetzold, Phys. Rev. B **42**, 56 (1990).  
<sup>11</sup>F. E. Bates, Phys. Rev. B **39**, 322 (1989).  
<sup>12</sup>T. Siegrist, S. Sunshine, D. W. Murphy, R. J. Cava, and S. M. Zahurak, Phys. Rev. B **35**, 7137 (1987).  
<sup>13</sup>T. Luty, J. Chem. Phys. **66**, 1231 (1977).  
<sup>14</sup>N. Neto, R. Righini, S. Califano, and S. H. Walmsley, Chem. Phys. **29**, 167 (1978).  
<sup>15</sup>P. G. Cummins, D. A. Dunmur, R. W. Munn, and R. J. Newham, Acta Crystallogr. A **32**, 847 (1976).  
<sup>16</sup>G. S. Pawley and J. W. Leech, J. Phys. C **10**, 2527 (1977).  
<sup>17</sup>S. L. Chaplot and K. R. Rao, J. Phys. C **16**, 3045 (1983).  
<sup>18</sup>W. H. Press, B. P. Flannery, S. A. Teukolsky, and W. T.

- Vetterling, *Numerical Recipes* (Cambridge University Press, Cambridge, 1986), p. 523.
- <sup>19</sup>A. Williams, G. H. Kwei, R. B. Von Dreele, A. C. Larson, I. D. Raistrick, and D. L. Bish, *Phys. Rev. B* **37**, 7960 (1988).
- <sup>20</sup>W. I. F. David, W. T. A. Harrison, J. M. F. Gunn, O. Moze, A. K. Soper, P. Day, J. D. Jorgensen, D. G. Hinks, M. A. Beno, L. Soderholm, D. W. Capone II, I. K. Schuller, C. U. Segre, K. Zhang, and J. D. Grace, *Nature* **327**, 310 (1987).
- <sup>21</sup>H. You, R. K. McMullan, J. D. Axe, D. E. Cox, J. Z. Liu, G. W. Crabtree, and D. J. Lam, *Solid State Commun.* **64**, 739 (1987).
- <sup>22</sup>W. Reichardt, N. Pyka, L. Pintschovius, B. Hennion, and G. Collin, *Physica C* **162-164**, 464 (1989).
- <sup>23</sup>J. R. Hardy and A. M. Karo, *The Lattice Dynamics and Statics of Alkali Halide Crystals* (Plenum, New York, 1979).
- <sup>24</sup>P. Brüesch and W. Bührer, *Z. Phys. B* **70**, 1 (1988).
- <sup>25</sup>M. Arai, K. Yamada, Y. Hidaka, S. Itoh, Z. A. Bowden, A. D. Taylor, and Y. Endoh, *Phys. Rev. Lett.* **69**, 359 (1992).